HHS Public Access

Author manuscript

Nat Commun. Author manuscript; available in PMC 2013 July 01.

Published in final edited form as:

Nat Commun. 2013 ; 4: 1798. doi:10.1038/ncomms2822.

FTO-Mediated Formation of N^6-Hydroxymethyladenosine and N^6-Formyladenosine in Mammalian RNA

Ye Fu[1,*], **Guifang Jia**[1,*], **Xueqin Pang**[2,3], **Richard N. Wang**[1], **Xiao Wang**[1], **Charles J. Li**[1], **Scott Smemo**[4], **Qing Dai**[1], **Kathleen A. Bailey**[4], **Marcelo A. Nobrega**[4], **Ke-li Han**[3], **Qiang Cui**[2], and **Chuan He**[1]

[1]Department of Chemistry and Institute for Biophysical Dynamics, The University of Chicago, 929 East 57th Street, Chicago, IL 60637, USA.

[2]Department of Chemistry and Theoretical Chemistry Institute, University of Wisconsin, Madison, WI 53706, USA.

[3]Dalian Institute of Chemical Physics, Chinese Academy of Sciences, Dalian, Liaoning, 116023, PR China.

[4]Department of Human Genetics, The University of Chicago, 920 E. 58th Street, Chicago, IL 60637, USA.

Abstract

N^6-methyladenosine (m^6A) is a prevalent internal modification in mRNA and non- coding RNA affecting various cellular pathways. Here we report the discovery of two additional modifications, N^6-hydroxymethyladenosine (hm^6A) and N^6- formyladenosine (f^6A), in mammalian mRNA. We show that Fe^{II}- and α-ketoglutarate (α-KG)-dependent fat mass and obesity associated (FTO) protein oxidizes m^6A to generates hm^6A as an intermediate modification and f^6A as a further oxidized product. hm^6A and f^6A have half-life times of ~3 h in aqueous solution under physiological relevant conditions, and are present in isolated mRNA from human cells as well as mouse tissues. These previously unknown modifications derived from the prevalent m^6A in mRNA, formed through oxidative RNA demethylation, may dynamically modulate RNA-protein interactions to affect gene expression regulation.

RNA modifications can affect molecular interaction and structural changes extending beyond local conformation of RNA. Not until recently were some of these modifications discovered to be reversible, dynamic, and responsive to cellular stimuli, which suggests that

Correspondence and requests for materials should be addressed to C.H. (chuanhe@uchicago.edu). . **Reprints and permission** information is available online at http://npg.nature.com/reprintsandpermissions/.

*These authors contributed equally to the work.

Author contributions Y.F., G.J., and C.H. designed and performed the experiments with the help of R.W., X.W., C.L., and Q.D., X.P., K.H., and Q.C. designed and performed the molecular dynamics (MD) simulations. K.B., S.S., and M.N. provided mouse tissue samples. Y.F., Q.C., and C.H. wrote the paper. All authors discussed the results and commented on the manuscript.

Supplementary Information accompanies this paper at http://www.nature.com/naturecommunications

Competing financial interests: The authors declare no competing financial interests.

they may participate in cellular regulatory processes[1,2]. N^6-methyladenosine (m^6A) is a widespread internal modification in mRNA, which constitutes 1-2% of all adenosine in mRNA[3]. Over 12,000 m^6A sites in the transcripts of more than 7,000 human genes have been characterized[4,5]. Conserved preference of m^6A around stop codons, in 3′-UTR, and within long internal exons have been revealed in both human and mouse cells[4,5]. This modification is essential to cell survival and development in eukaryotes, and plays a fundamental role in gene expression regulation[6,7]. While the methyltransferase complex is thought to contain METTL3 in mammals[8], the following have been identified as components of this complex in yeast: Ime4 (yeast m^6A methyltransferase), Mum2, and Slz1[9]. We have discovered that the human fat mass and obesity-associated protein FTO catalyzes the removal of m^6A *in vitro* and *in vivo*, providing the first example of reversible methylation in RNA[2]. FTO, which was identified in several genome-wide-association studies to be associated with obesity and Type II diabetes[10-12], is a member of the non-heme Fe^{II}/α-ketoglutarate (α-KG)-dependent AlkB family demethylases that mainly catalyze oxidative demethylation of *N*-alkylated nucleic acid bases[13-15].

We seek to further understand the FTO-mediated oxidative demethylation of m^6A (Fig. 1a) and identify potential new modifications that could be present inside mammalian cells since this family of enzymes exhibits versatile activities[16]. For instance, the recently discovered TET enzymes that belong to the general family of non-heme Fe^{II}/α-KG-dependent dioxygenases can perform tandem oxidations[17-20]. Initially shown to catalyze the oxidation of 5-methylcytosine (5mC) to 5-hydroxymethylcyotosine (5hmC) in mammalian genomic DNA[17, 18], TET proteins were found to further oxidize 5hmC to 5-formylcytosine (5fC) and 5-carboxylcytosine (5caC)[19-21]. 5hmC levels are highest in brain extracts and 5hmC is thought to be a new DNA epigenetic marker[22]. The oxidation of 5hmC to 5fC and/or 5caC is a much slower process compared to the oxidation of 5mC to 5hmC[20]. Nevertheless, the continuous oxidation of 5hmC by TET enzymes is essential to an active DNA demethylation pathway, and plays important roles in regulating DNA epigenetics[19, 23].

Here we show that FTO oxidizes m^6A to hm^6A and f^6A in RNA in a step-wise manner. The observation is further supported by molecular dynamic simulation, which indicates that FTO can bind to hm^6A as well as m^6A as substrates. We further demonstrate that hm^6A and f^6A are relatively stable under physiological conditions and can be detected in polyadenylated RNA isolated from human cells and mouse tissues. These meta-stable intermediates, generated during the course of the FTO-catalyzed m^6A demethylation and discovered for the first time inside mammalian cells, may have significant functional implications.

Results

New modifications in the FTO–mediated m^6A oxidation

In order to investigate the FTO-catalyzed demethylation process, we monitored the reaction with high-resolution MALDI-TOF/TOF mass spectrometry to detect N^6-hydroxymethyladenosine (hm^6A), an expected oxidation product of m^6A in RNA by FTO. 5 uM of 9mer single-stranded RNA (ssRNA) containing m^6A was treated with 10 uM of FTO at room temperature for 20 min, and analyzed immediately after reaction (Fig. 1b). To our surprise, when analyzing the monoisotopic peaks, other than the peak of demethylation

product (m^6A-14 Da), we also observed another m^6A+14 Da peak representing an unknown reaction product (Fig. 1b). The putative hm^6A product has a molecular weight of m^6A+16 Da, which likely loses a H_2O moiety (-18 Da) to form N^6-methyleneadenosine (m^6A −2 Da) during the process (Fig. 1b). We speculated that this unexpected +14 Da peak may correspond to N^6-formyladenosine (f^6A) as a result of a tandem oxidation of the m^6A substrate in a process similar to that of the oxidation of 5mC to 5hmC and 5fC by the TET proteins in the DNA demethylation pathway. Since the oxidation of hemiaminal to amide is a rare chemical transformation, and the enzymatic conversion of this process has never been reported, we proceeded to further confirm the identity of this unprecedented species.

We reasoned that in previous HPLC analysis of the digested nucleosides, the basic conditions used during alkaline phosphatase digestion may accelerate the hydrolysis of this reaction product[2]. Since FTO showed similar demethylation activity between internal and terminal m^6A in RNA (Fig. 1b and Supplementary Fig. S1), we synthesized a 9mer ssRNA oligonucleotide with m^6A incorporated at the 5′ end for further studies. In this case, we could analyze the first nucleoside at the 5′ position with only nuclease P1 digestion in order to avoid the basic conditions (Fig. 2a). 5 uM of the substrate RNA was treated with 2.5 uM of FTO for 2 min or 20 min at room temperature, and the reaction product was digested with Nuclease P1 and run through a C18 reverse phase column on HPLC. Two new peaks other than m^6A and A were observed (Fig. 2b). We suspected that the initially generated product was N^6-hydroxymethyladenosine (hm^6A), and the latter product was N^6-formyladenosine (f^6A).

To confirm the identities of these species, we chemically synthesized hm^6A and f^6A standards following reported procedures (Supplementary Methods and Supplementary Fig. S2)[24, 25]. Briefly, after treating 100 uM of adenosine with 30 mM of formaldehyde at 60 °C for 4 h, hm^6A was produced, which partially dehydrated to N^6- methylene-adenosine in equilibrium (Supplementary Fig. S2a)[24]. f^6A could be prepared by treating *N*,*N*-dimethylformamidine-protected TBDMS-adenosine with weak acid *N*-hydroxybenzotriazole ($HOBt{\cdot}H_2O$) in MeOH (Supplementary Fig. S2b), followed by deprotection of the TBDMS group[25]. f^6A is stable in dry organic solvent, and can be further characterized by HRMS, NMR, and UV-Vis spectra analysis (Supplementary Fig. S3 and S4). It has the highest absorbance at 274 nm with $\varepsilon_{max(274nm)} = 1.83\times10^4$ (Supplementary Fig. S4) in water.

The two reaction products co-elute with synthesized hm^6A and f^6A standards in HPLC (Fig. 2b), and have the same MS/MS fragmentation pattern as hm^6A (Fig. 2c) and f^6A (Fig. 2d), respectively, thus confirming their identities. Both hm^6A and f^6A decompose to A in aqueous solution, and the hydrolysis processes were accelerated under acidic or basic conditions (Supplementary Fig. S5). To measure the stability of hm^6A and f^6A under physiological conditions, hm^6A- and f^6A-containing RNA generated by FTO oxidation *in situ* were digested with Nuclease P1, and diluted in buffer solutions mimicking the physiological conditions with Tris-HCl (20 mM, pH 7.4), KCl (140 mM), NaCl (15 mM), and $MgCl_2$ (1 mM). The solutions were incubated at 37 °C, and analyzed by HPLC-MS/MS to monitor the degradation process. In the neutral buffered solution, long half-life times of 186 ± 25 min for hm^6A and 188 ± 18 min for f^6A were observed, respectively

(Supplementary Fig. S6), which are comparable to the average half-life of mRNA in mammalian cells[26]. The relative long life times of hm^6A and f^6A under physiological conditions suggest that they are present inside living cells and may have functional roles other than as mere demethylation intermediates.

Reaction kinetics of FTO-mediated oxidation

To elucidate the kinetic behavior of the production of hm^6A and f^6A, we measured a time-course reaction profile of FTO (2.5 uM) on the same RNA (5 uM) at 37 °C by quantitative LC-MS/MS (Fig. 2e and Supplementary Fig. S7). We found that similar to the oxidation of 5mC to 5hmC and then 5fC by Tet[20], FTO catalyzes the oxidation of hm^6A to f^6A at a relatively slower rate compared to the oxidation of m^6A to hm^6A (Fig. 2e). The kinetic behavior of this two-step oxidation process suggests a non-processive oxidation pathway, which involves the releasing and rebinding of the hm^6A intermediate to the FTO active site. Generation of f^6A will be sensitive to the FTO concentration as the two-step reaction harbors a fast first step and a slow second step; higher local concentrations of FTO will result in the production of more f^6A.

FTO recognizes m^6A as well as hm^6A as its substrate

To further rationalize our observations we used Molecular Dynamics (MD) simulation to model the binding of FTO with m^6A and hm^6A. Protein coordinates were retrieved from the crystal structure of FTO-N^3-methylthymine (m^3T) complex (PDB ID: 3LFM)[27]; initial base coordinates were set up in two independent ways. The first approach was to fix the sugar ring position of m^3T in 3LFM, and mutate m^3T to N^3-methylcytosine (m^3C), m^6A, and hm^6A. These systems were labeled as FTO-m^3T-cry, FTO-m^3C-cry, FTO-m^6A-cry, and FTO-hm^6A-cry, respectively. The second protocol involves aligning the AlkB-DNA complex crystal structures with FTO based on similarities in protein structure calculated with the Protein Comparison Tool[28] (Supplementary Fig. S8 and S9) and then using the coordinates of the lesioned bases from the aligned AlkB complexes[29]. We used PDB file 3O1O to derive the coordinates for m^3T, 3O1M for m^3C, and 3O1P for εA, respectively; εA was then mutated to m^6A or hm^6A. These systems were labeled as FTO-m^3T-alkb, FTO-m^3C-alkb, FTO-m^6A-alkb, and FTO-hm^6A-alkb, respectively (Supplementary Fig. S10).

We calculated the binding models of m^6A (Supplementary Fig. S11 and S12) and hm^6A (Supplementary Fig. S13 and S14) in FTO with more than 10 ns MD simulation, in comparison with m^3T (Supplementary Fig. S15 and S16) and m^3C (Supplementary Fig. S17 and S18) (Supporting methods). Similar to m^3T, both m^6A (Fig. 3a) and hm^6A (Fig. 3b) are stable in the active site in two sets of MD simulations using two initial positions retrieved by two independent methods described above (Left panels were calculated using the FTO-m^3T crystal structure to prepare the initial coordinates of the base; right panels were calculated using aligned AlkB crystal structures to derive the initial base coordinates.). Overlays of these structures with the FTO-m^3T crystal structure show that N^6-methyl in m^6A (Fig. 3c) and N^6-methylene in hm^6A (Fig. 3d) position near the iron center in the active site of FTO similar to N^3-methyl in m^3T in the solved structure[27]. As a negative control, m^3C was observed to be unstable in FTO and dissociated from the active site after 3 ns of simulation

(Supplementary Fig. S17 and S18), which was likely the result of the positive charge of m^3C.

Relative binding free energies of m^6A and hm^6A to FTO were also calculated by alchemical free energy simulations[30] (Supplementary Methods, Supplementary Fig. S19 and S20). All independent simulations predicted a slightly stronger binding (ranging from 0.4 to 2.8 kcal/mol) for hm^6A over m^6A (Supplementary Table S1). This data supports our observation of hm^6A as a substrate for FTO, and suggests a similar oxidation model of m^6A to hm^6A for hm^6A to f^6A, in agreement with the kinetic behavior of the oxidation reaction and a proposed non-processive tandem oxidation reaction pathway.

Detection of hm^6A and f^6A in human and mouse mRNA

In order to confirm the existence of these new modifications *in vivo*, we optimized RNA digestion conditions using RNase T1 followed by Nuclease P1 at neutral pH, in which both hm^6A and f^6A are relatively stable. RNase T1 cleaves the phosphodiester bond after G, and exposes the following nucleotide with a free 5′-OH. Nuclease P1 releases this nucleotide for subsequent HPLC separation (Fig. 4a). While m^6A shows a preference in the consensus sequence of [G/A/U][G>A]m^6AC[U>A>C][4,5], this method can analyze hm^6A and f^6A present in this consensus sequence after G. Applying this method we analyzed the isolated poly(A)-RNA from cultured HeLa cells and mouse liver tissues by LC-MS/MS. We observed peaks with the same elution times at the MS/MS detection channel of hm^6A (298.1 fragmented to 136.0, Fig. 4b) and f^6A (296.1 fragmented to 164.1, Fig. 4c), respectively. We subsequently followed the f^6A peak, which is more stable than hm^6A. f^6A in mouse liver decreased significantly upon incubating at room temperature overnight (Supplementary Fig. S21), similar to that observed with the f^6A standard. Therefore, we confirmed the presence of hm^6A and f^6A in poly(A)-RNA *in vivo*. The concentration of the isolated f^6A (a large portion of f^6A may have decomposed during the isolation process) was estimated to be at least 0.5-1% of the total m^6A (Supplementary Fig. S22). A similar amount of hm^6A appears to also exist *in vivo* based on our results. Therefore, taking account of decomposition during isolation a noticeable portion of mRNA should carry either hm^6A or f^6A at any given time inside cells.

hm^6A and f^6A may modulate RNA-protein interactions

Since the oxidation of 5mC to 5hmC and then 5fC in DNA hinders binding to methyl-CpG-binding (MBD) proteins[31], we envisioned that the extra oxygen group on hm^6A and f^6A may hinder their interaction with m^6A-binding proteins. Recently, YTHDF proteins have been implicated as potential m^6A-RNA binding proteins[4]. To evaluate its binding affinity to these RNA modifications, we cloned and expressed a GST-tagged YTHDF2 protein. The binding affinities of YTHDF2 to RNA containing hm^6A or f^6A, generated *in situ* by FTO-mediated oxidation, were measured and compared to those with m^6A or A using electrophoretic mobility shift assay (EMSA) (Supplementary Fig. S23). About 70% of hm^6A (Supplementary Fig. S24) and 60% of f^6A (Supplementary Fig. S25) were estimated to be present in the EMSA assay, respectively, as shown by LC-MS/MS analysis of an unlabeled 9mer RNA that contained 5′-m^6A treated using the same procedure. We found that the YTHDF2 protein preferentially binds to m^6A-RNA as a well-shifted band with an

apparent K_d of 465 ± 16 nM, while the binding affinities of YTHDF2 to hm^{6}A or f^{6}A were attenuated to a level similar to A (Supplementary Fig. S23).

Discussion

We show here that *N*^{6}-hydroxymethyladenosine and *N*^{6}-formyladenosine are new RNA modifications in mammalian cells, and that FTO can catalyze the formation of these modifications. The AlkB protein has been shown to oxidize m^{6}A to hm^{6}A as an oxidation intermediate *in vitro* with no further oxidation of hm^{6}A observed[32]. FTO shows the unique activity of performing a second oxidation on the meta-stable hm^{6}A to form an unprecedented f^{6}A. Compared to other hemiaminal intermediates, hm^{6}A is relatively stable due to the electron-rich nature of the exocyclic *N*^{6} nitrogen of adenosine when compared to endocyclic positions, which allows for further oxidation to f^{6}A.

Although more than one hundred RNA modifications have been discovered, the chemical diversity of the modifications is relatively limited. Recent application of more sensitive analytical methods leads to the discovery of RNA modifications with novel functional groups, such as geranylated RNA in bacteria[33]. The discovery of hydroxymethylated and formylated adenosines in mRNA here further expands the repertoire of chemical diversity of RNA modifications. As m^{6}A has not only been detected in mRNA but also long non-coding RNA, it is possible that hm^{6}A and f^{6}A which are derived from m^{6}A may also exist in long non-coding RNAs. FTO exhibits a relatively high activity towards m^{6}A on single-stranded RNA, but lower activity towards m^{6}A in stem-loop structures and negligible activity against m^{6}A on double-stranded RNA *in vitro*[2]. The in vivo activity could be affected by the secondary structure of the RNA and cellular machineries that recruit FTO to specific RNA substrates.

FTO and the methyltransferase components orchestrate together to determine the modification status of mRNA. As FTO is partially localized in nuclear speckles[2], in which the methyltransferase complex resides, the demethylated RNA could be re-methylated by the methyltransferase in a direct reversible model. In contrast, the temporary existence of the hydroxymethyl and the formyl group on the *N*^{6} position of adenosine may represent a delayed reversible model, in which an additional diffusion/export step may be incorporated and coupled with the “slow” hydrolysis step (Fig. 5). Therefore, these meta-stable intermediates could provide a time-window for the oxidized RNA to diffuse or be exported out of the nuclear speckles, thus eliminating the possibility of re-methylation by the methyltransferase complex at the same loci *in vivo* (Fig. 5). It is also interesting to speculate about other functional roles of hm^{6}A and f^{6}A because they are not recognized by m^{6}A-binding proteins such as YTHDF2. They could serve as another modification marker to recruit different sets of RNA-binding proteins, and differentially regulate the subsequent RNA-related pathways (Fig. 5), or they could serve as markers for nascent RNAs taking advantage of their intrinsic degradation kinetics. It is also interesting to note that the FTO-mediated formation of hm^{6}A and f^{6}A is similar to the TET-mediated oxidation of 5mC to 5fC and 5caC in DNA[19-21]. While hm^{6}A and f^{6}A are inherently unstable, it is possible that additional protein factors could be involved to promote the FTO-mediated demethylation of m^{6}A by catalyzing the hydrolysis of hm^{6}A and f^{6}A; on the other hand, hm^{6}A and f^{6}A can

also be stabilized when buried in a hydrophobic environment of their potential binding proteins. Further studies to explore the potential functions of these two modifications are required in the future to address these hypotheses.

In summary, the identification of hm^{6}A and f^{6}A in cellular mRNA shows that additional modifications can be installed onto the N^6-position of adenosine, which impact protein-RNA interaction to perhaps provide further dynamical tuning of the function/status of mRNA. Therefore, the discovery of these additional modifications on mRNA presents many intriguing questions and new biology to be explored.

Methods

General materials and methods

cDNA clone of full-length human FTO and YTHDF2 was purchased from Open Biosystems. All primers were purchased from Eurofins MWG Operon. All RNase-free solutions were prepared from DEPC-treated MilliQ-water.

Synthesis and characterization of synthetic f^6 A standard

Detailed description of the synthesis of f^{6}A standard can be found in the Supplementary Methods. The f^{6}A standard was characterized by HPLC-QQQ-MS/MS, high-resolution mass spectra, UV-Vis spectra, and both ^{1}H and ^{13}C NMR (Supplementary Fig. S2–S4). Characterization data of f^{6}A: ^{1}H NMR (DMSO-d_6, 500 MHz) δ11.395 (br, 1H), 9.953 (s, 1H), 8.766 (s, 1H), 8.617 (s, 1H), 6.034 (d, J = 5.5 Hz, 1H), 5.574 (d, J = 6.0 Hz, 1H), 5.278 (d, J = 5.0 Hz, 1H), 5.185 (t, J = 5.5 Hz, 1H), 4.625 (dd, J = 5.5 Hz, 5.5 Hz, 1H), 4.202 (dd, J = 5.0 Hz, 4.0 Hz, 1H), 4.001 (dd, J = 3.5 Hz, 4.0 Hz, 1H) 3.713 (m, 1H), 3.607 (m, 1H) ppm; ^{13}C NMR (DMSO-d_6, 125 MHz) 165.193, 152.995, 152.649, 150.665, 144.237, 122.245, 88.690, 86.697, 74.769, 71.239, 62.204 ppm. UV/Vis: λ_{max},274nm, $\varepsilon_{(260\ nm)}$ = 1.30×10^4 M^{-1} cm^{-1}, $\varepsilon_{max(274\ nm)}$ = 1.83×10^4 M^{-1} cm^{-1}, LC-QQQ-MS/MS (Positive): $[M+H]^+$ = 296.1, $[Base+H]^+$ = 164.0, HRMS (m/z) for $C_{11}H_{13}N_5O$ $[M+H]^+$ 5: = 296.0995 (calcd.), 296.1009 (found).

Synthesis of m^6 A-RNA oligo

m^{6}A phosphoramidite (N^6-methyl-5′-*O*-(4,4′- dimethoxytrityl)-2′-*O*-t-butyldimethylsilyl adenosine 3′-*O*-(2-cyanoethyl-*N*,*N*-diisopropyl)phosphoramidite) was synthesized according to a previously reported procedure[34]. RNA oligo containing m^{6}A was synthesized using m^{6}A RNA phosphoramidite and standard RNA phosphoramidite (Glen Research) under ultra-mild conditions using 1H-tetrazole as activator reagent in an Expedite^{TM} Nucleic Acid Synthesis System (PerSeptive Biosystems) with DMT-ON protocol. The oligo was cleaved from the beads and purified in a Glen-Pak^{TM} RNA purification cartridge (Glen Research) according to the standard protocol provided by the manufacturer. The quality and purity of synthesized RNA was monitored by high resolution MALDI-TOF-MS. Synthesized RNA sequence: RNA oligo with internal m^{6}A: CUGGm^{6}ACUGG, RNA oligo with 5′ m^{6}A: m^{6}ACUGACUAG.

Biochemistry assay of FTO activity *in vitro*

N-terminal his-tagged truncated human FTO protein (his_6-FTO-NΔ31) was expressed and purified as previously reported[27]. The demethylation activity assay was performed in 20 μl to 100 μl of reaction mixture containing RNA with m^6A, FTO, 75 μM of $(NH_4)_2Fe(SO_4)_2{\cdot}6H_2O$, 300 μM of α-KG, 2 mM of L-ascorbic acid, 150 mM of KCl, and 50 mM of HEPES buffer (pH 7.0). The reaction was incubated at room temperature or 37 °C, and quenched by the addition of 1 mM of EDTA. The reaction was then frozen in liquid N_2 immediately, and thawed only before analysis was performed. For HPLC or HPLC-MS/MS analysis, the reaction mixture was digested by 1 U of nuclease P1 at 37 ° C for 15 min. HPLC analysis was performed on a HPLC system equipped with an Agilent Eclipse XDB-C18 analysis column (150×4.6 mm) eluted with buffer A (50 mM ammonium acetate in H_2O) and buffer B (50 mM ammonium acetate in 60% of acetonitrile in H_2O) with a flow rate of 1 ml min^{-1} at room temperature. The detection wavelength was set at 260 nm and 280 nm. HPLC-MS/MS was carried out by reverse-phase ultra-performance liquid chromatography on an Agilent ZORBAX Eclipse XDB-C18 column (Rapid Resolution HT, 50×2.1 mm) eluted with buffer A (0.1% formic acid in H_2O) and buffer B (0.1% formic acid in methanol) with a flow rate of 0.5 ml min^{-1} at 35 °C, with online mass spectrometry detection using Agilent 6410 triple-quadrupole (QQQ) LC mass spectrometer in multiple reaction monitoring (MRM) positive electrospray ionization (ESI) mode. The nucleosides were quantified using the nucleoside to base ion mass transitions of 282.1 to 150.1 (m^6A), 268.0 to 136.0 (A), 296.1 to 164.1 (f^6A), and 198.1 to 136.1 (hm^6A). Quantification was performed by comparison with the standard curve obtained from synthetic nucleoside standards running at the same batch of samples.

MALDI-TOF-MS analysis of RNA oligo

The RNA/FTO reaction solution was first desalted by mixing with 50 uL of ammonium-charged AG 50W-X8 Cation Exchange Resins (Biorad). 1 uL of the desalted solution was then mixed with an equal amount of MALDI matrix, which was composed by 9:1 (v:v) ratio of 2′,4′,6′ trihydroxyacetophenone (THAP, 10 mg/mL in 50% CH_3CN/H_2O):diammonium citrate (50 mg/mL in H_2O). The mixture was then spotted on a MALDI sample plate, dried under vacuum, and analyzed by a Bruker Ultraflextreme MALDI-TOF-TOF Mass Spectrometers in reflector, positive mode.

Analysis of hm^6A and f^6A in mRNA using HPLC-MS/MS

Total RNA was isolated from cultured cell or mouse tissues using TRIzol® reagent according to the manufacture procedure. mRNA was then isolated with biotin-oligo(dT) and streptavidin beads from Promega, following a modified procedure, which eliminated all heating steps. 8 ug of mRNA was digested with RNase T1 in 20 uL for 15 min at 37 °C, followed by nuclease P1 (1 U) for 30 min at 37 °C. The solution was diluted 5 times, and 20 μl of the solution was analyzed by HPLC-QQQ-MS/MS. The nucleosides were quantified using the nucleoside to base ion mass transitions of 282.1 to 150.1 (m^6A), 268.0 to 136.0 (A), 296.1 to 164.1 (f^6A), and 198.1 to 136.1 (hm^6A) in MRM positive ESI mode.

MD and alchemical free energy simulations

The initial coordinates were taken from the crystal structure of FTO bound with Fe^{2+}, *N*-oxalyglycine and m^3T (PDB ID: 3LFM). We replaced the N-oxalyglycine (antagonist of FTO) with the active co-factor α- ketoglutarate (α-KG). The coordinates of the modified bases were generated in two different ways, and two independent sets of simulations were carried out accordingly. The first approach was to fix the sugar ring position of m^3T in 3LFM, and then mutate the original m^3T to m^3C, m^6A or hm^6A, respectively. These systems were labeled as FTO- m^3T-cry, FTO-m^3C-cry, FTO-m^6A-cry and FTO-hm^6A-cry, respectively. The second protocol was to align the AlkB-DNA complex crystal structures with FTO based on 3D protein structure similarity calculated with the Protein Comparison Tool and then take the coordinates of the modified bases from the aligned AlkB complexes. We used PDB file 3O1O to derive the coordinates for m^3T, 3O1Mfor m^3C, and 3O1Pfor εA; εA was then mutated to m^6A or hm^6A. These systems were labeled as FTO-m^3T-alkb, FTO-m^3C-alkb, FTO-m^6A-alkb and FTO-hm^6A-alkb, respectively. Detailed procedure for MD simulation setup and alchemical free energy simulations for relative binding affinities are provided in Supplementary Methods.

Supplementary Material

Refer to Web version on PubMed Central for supplementary material.

Acknowledgments

We thank Dr. Q. Jin for help with MALDI-TOF-MS and HPLC-QQQ-MS/MS, and G. Hou for discussions of technical issues on MD simulations. This work is supported by National Institute of Health (GM071440 to C.H., and GM084028 to Q.C.) and by a NIH EUREKA award (GM088599 to C.H.). The Mass Spectrometry Facility of the University of Chicago is funded by National Science Foundation (CHE-1048528). Y.F. is supported by Weil Endowed Fellowship. Y.F. and X.P. acknowledges support from the China Scholarship Council. We thank S. F. Reichard, MA for editing the manuscript.

References

1. Chan CT, et al. A quantitative systems approach reveals dynamic control of tRNA modifications during cellular stress. PLoS Genet. 2010; 6:e1001247. [PubMed: 21187895]
2. Jia G, et al. N6-Methyladenosine in nuclear RNA is a major substrate of the obesity-associated FTO. Nat. Chem. Biol. 2011; 7:885–887. [PubMed: 22002720]
3. Perry RP, Kelley DE, Friderici K, Rottman F. The methylated constituents of L cell messenger RNA: evidence for an unusual cluster at the 5′ terminus. Cell. 1975; 4:387–394. [PubMed: 1168101]
4. Dominissini D, et al. Topology of the human and mouse m6A RNA methylomes revealed by m6A-seq. Nature. 2012; 485:201–206. [PubMed: 22575960]
5. Meyer KD, et al. Comprehensive Analysis of mRNA Methylation Reveals Enrichment in 3′ UTRs and near Stop Codons. Cell. 2012; 149:1635–1646. [PubMed: 22608085]
6. Bodi Z, Button JD, Grierson D, Fray RG. Yeast targets for mRNA methylation. Nucleic. Acids. Res. 2010; 38:5327–5335. [PubMed: 20421205]
7. Hongay CF, Orr-Weaver TL. Drosophila Inducer of MEiosis 4 (IME4) is required for Notch signaling during oogenesis. Proc. Natl. Acad. Sci. U. S. A. 2011; 108:14855–14860. [PubMed: 21873203]
8. Bokar JA, Shambaugh ME, Polayes D, Matera AG, Rottman FM. Purification and cDNA cloning of the AdoMet-binding subunit of the human mRNA (N6-adenosine)- methyltransferase. RNA. 1997; 3:1233–1247. [PubMed: 9409616]

9. Agarwala SD, Blitzblau HG, Hochwagen A, Fink GR. RNA Methylation by the MIS Complex Regulates a Cell Fate Decision in Yeast. PLoS Genet. 2012; 8:e1002732. [PubMed: 22685417]
10. Dina C, et al. Variation in FTO contributes to childhood obesity and severe adult obesity. Nat. Genet. 2007; 39:724–726. [PubMed: 17496892]
11. Frayling TM, et al. A common variant in the FTO gene is associated with body mass index and predisposes to childhood and adult obesity. Science. 2007; 316:889–894. [PubMed: 17434869]
12. Scuteri A, et al. Genome-wide association scan shows genetic variants in the FTO gene are associated with obesity-related traits. PLoS Genet. 2007; 3:e115. [PubMed: 17658951]
13. Falnes PO, Johansen RF, Seeberg E. AlkB-mediated oxidative demethylation reverses DNA damage in Escherichia coli. Nature. 2002; 419:178–182. [PubMed: 12226668]
14. Trewick SC, Henshaw TF, Hausinger RP, Lindahl T, Sedgwick B. Oxidative demethylation by Escherichia coli AlkB directly reverts DNA base damage. Nature. 2002; 419:174–178. [PubMed: 12226667]
15. Gerken T, et al. The obesity-associated FTO gene encodes a 2-oxoglutarate-dependent nucleic acid demethylase. Science. 2007; 318:1469–1472. [PubMed: 17991826]
16. Loenarz C, Schofield CJ. Physiological and biochemical aspects of hydroxylations and demethylations catalyzed by human 2-oxoglutarate oxygenases. Trends Biochem. Sci. 2011; 36:7–18. [PubMed: 20728359]
17. Kriaucionis S, Heintz N. The nuclear DNA base 5-hydroxymethylcytosine is present in Purkinje neurons and the brain. Science. 2009; 324:929–930. [PubMed: 19372393]
18. Tahiliani M, et al. Conversion of 5-methylcytosine to 5-hydroxymethylcytosine in mammalian DNA by MLL partner TET1. Science. 2009; 324:930–935. [PubMed: 19372391]
19. He YF, et al. Tet-mediated formation of 5-carboxylcytosine and its excision by TDG in mammalian DNA. Science. 2011; 333:1303–1307. [PubMed: 21817016]
20. Ito S, et al. Tet proteins can convert 5-methylcytosine to 5-formylcytosine and 5-carboxylcytosine. Science. 2011; 333:1300–1303. [PubMed: 21778364]
21. Pfaffeneder T, et al. The discovery of 5-formylcytosine in embryonic stem cell DNA. Angew. Chem. Int. Ed. Engl. 2011; 50:7008–7012. [PubMed: 21721093]
22. Munzel M, et al. Quantification of the sixth DNA base hydroxymethylcytosine in the brain. Angew. Chem. Int. Ed. Engl. 2010; 49:5375–5377. [PubMed: 20583021]
23. Zhang L, et al. Thymine DNA glycosylase specifically recognizes 5-carboxylcytosine-modified DNA. Nat. Chem. Biol. 2012; 8:328–330. [PubMed: 22327402]
24. Alderson T. Mechanism of formaldehyde-induced mutagenesis. The uniqueness of adenylic acid in the mediation of the mutagenic activity of formaldehyde. Nature. 1960; 187:485–489.
25. Ohkubo A, et al. Oligonucleotide synthesis involving deprotection of amidine-type protecting groups for nucleobases under acidic conditions. Org. Lett. 2010; 12:2496–2499. [PubMed: 20455549]
26. Ross J. mRNA stability in mammalian cells. Microbiol. Rev. 1995; 59:423–450. [PubMed: 7565413]
27. Han Z, et al. Crystal structure of the FTO protein reveals basis for its substrate specificity. Nature. 2010; 464:1205–1209. [PubMed: 20376003]
28. Prlic A, et al. Pre-calculated protein structure alignments at the RCSB PDB website. Bioinformatics. 2010; 26:2983–2985. [PubMed: 20937596]
29. Yi C, et al. Iron-catalysed oxidation intermediates captured in a DNA repair dioxygenase. Nature. 2010; 468:330–333. [PubMed: 21068844]
30. Straatsma TP, Mccammon JA. Multiconfiguration thermodynamic integration. J. Chem. Phys. 1991; 95:1175–1188.
31. Hashimoto H, et al. Recognition and potential mechanisms for replication and erasure of cytosine hydroxymethylation. Nucleic. Acids. Res. 2012; 40:4841–4849. [PubMed: 22362737]
32. Li D, et al. Exocyclic carbons adjacent to the N(6) of adenine are targets for oxidation by the Escherichia coli adaptive response protein AlkB. J. Am. Chem. Soc. 2012; 134:8896–8901. [PubMed: 22512456]

33. Dumelin CE, Chen Y, Leconte AM, Chen YG, Liu DR. Discovery and biological characterization of geranylated RNA in bacteria. Nat. Chem. Biol. 2012; 8:913–919. [PubMed: 22983156]

34. Dai Q, et al. Identification of recognition residues for ligation-based detection and quantitation of pseudouridine and N6-methyladenosine. Nucleic Acids Res. 2007; 35:6322–6329. [PubMed: 17881375]

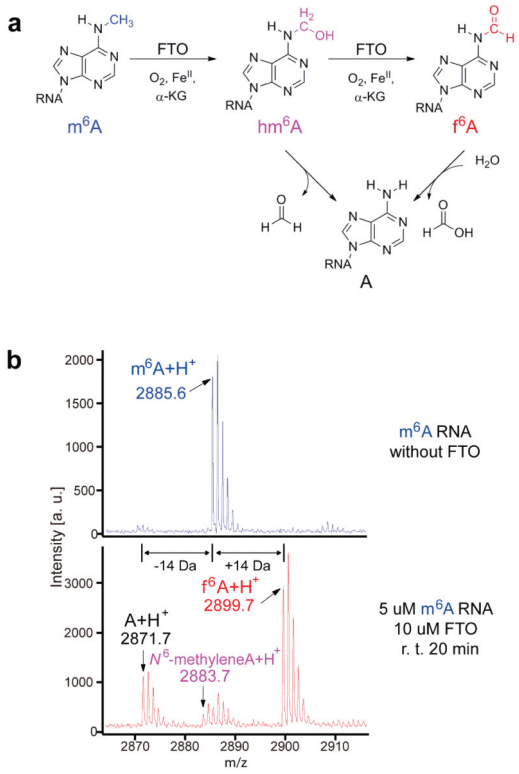

Figure 1. Oxidative demethylation of m^6 A in RNA by FTO

(**a**) FTO demethylates m^{6}A through oxidization of m^{6}A to hm^{6}A with f^{6}A as a further oxidized product. (**b**) MALDI-TOF analysis of m^{6}A-RNA after reacting with FTO. An unexpected monoisotopic peak of m^{6}A+14 Da corresponding to f^{6}A was observed after treating a 9mer m^{6}A-RNA oligo (5 uM) with 10 uM of FTO at room temperature for 20 min. The m^{6}A-2 Da peak represents the dehydration product of the putative hm^{6}A intermediate during MALDI-TOF ionization.

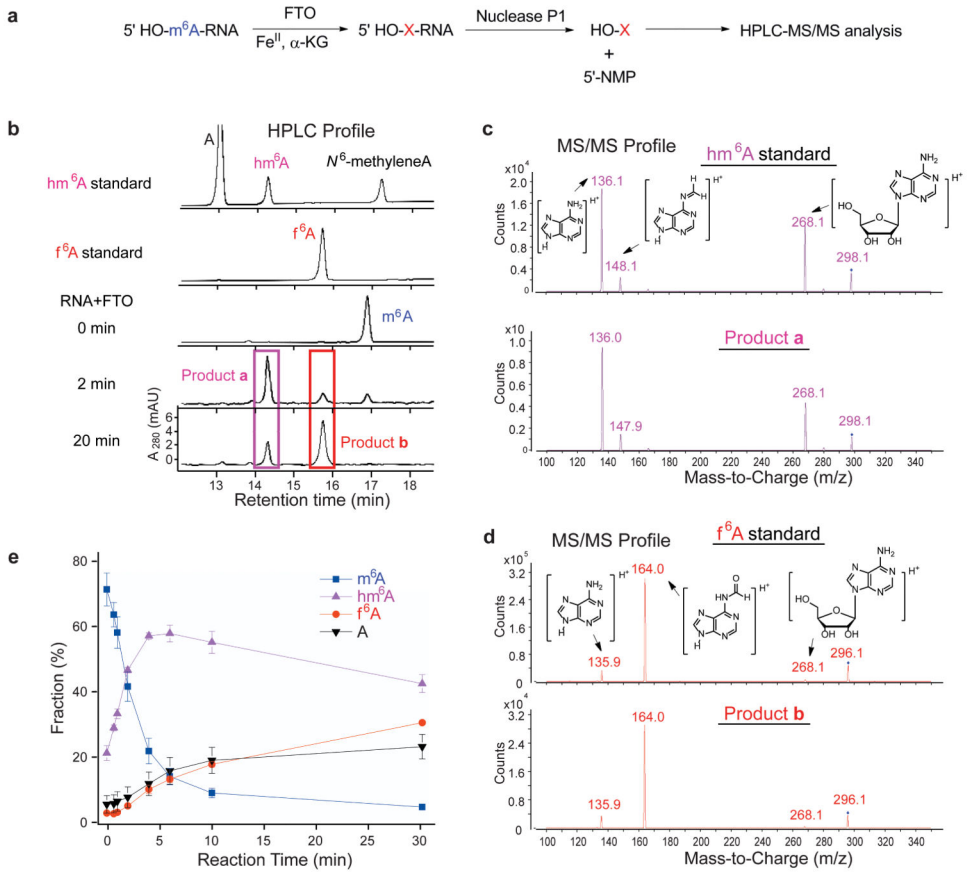

Figure 2. Formation of new RNA modifications during oxidative demethylation of m^6 A in RNA by FTO

(**a**) A 9mer ssRNA containing a 5′ m^{6}A is used for HPLC-MS/MS analysis. After the RNA is treated with FTO, it is digested by Nuclease P1 to release the first base as a nucleoside for further HPLC-MS/MS analysis. The rest of the bases are left as nucleoside 5′-monophosphate (5′-NMP). (**b**) HPLC analysis of Nuclease P1-digested 5′m^{6}A-9mer RNA oligo (5 uM) after treating with FTO. m^{6}A was converted to hm^{6}A and f^{6}A after the treatment with 2.5 uM of FTO for 2 min at room temperature; substantial conversion of hm^{6}A to f^{6}A can be observed in 20 min. These newly formed peaks co-elute with hm^{6}A and f^{6}A standards, respectively. The last peak in hm^{6}A standard is *N*^{6}-methyleneadenosine, a dehydration product that co-exists with hm^{6}A. (**c, d**) Comparison of MS/MS profile of m^{6}A-oxidation products with hm^{6}A and f^{6}A standards. (**c**) The initial product matches the elution time and MS/MS fragmentation pattern of hm^{6}A. (**d**) The later-formed product matches the elution time and MS/MS fragmentation pattern of f^{6}A. (**e**) Kinetic behavior of the reaction indicates that the formation rate of f^{6}A is slower than the oxidation rate from m^{6}A to hm^{6}A by a factor of 12.3 ± 1.9. Error bars, mean ± s.e.m. for n = 4 experiments.

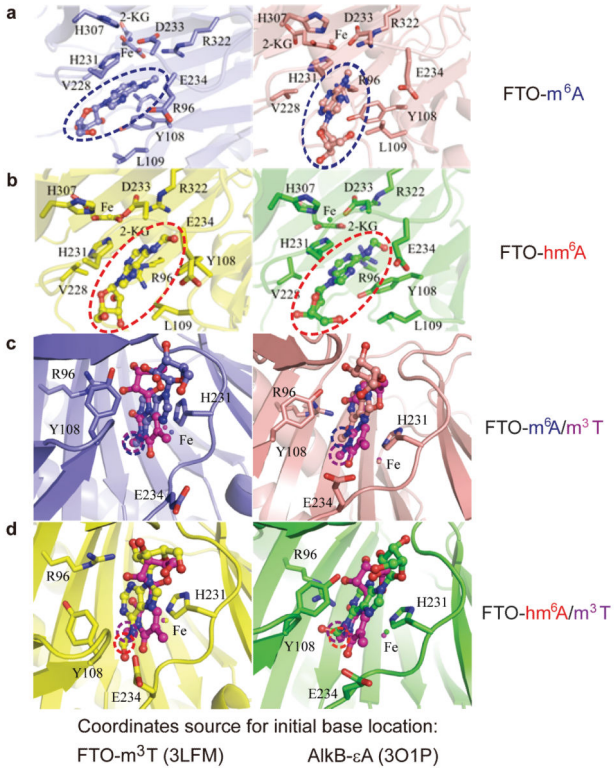

Figure 3. Simulated binding mode of m^6 A and hm^6 A in FTO after 10 ns of Molecular Dynamic (MD) simulations

(**a**) Binding model of FTO-m^{6}A. (**b**) Binding model of FTO-hm^{6}A. m^{6}A and hm^{6}A is highlighted in dashed blue and red circles. (**c**) Binding model comparison of m^{6}A overlay with m^{3}T. (**d**) Binding model comparison of hm^{6}A overlay with m^{3}T. Positions of the targeting methyl in m^{6}A and hm^{6}A are highlighted in dashed blue and red circles, respectively; the targeting methyl in m^{3}T is highlighted in dashed magenta circles. Protein structure is shown in cartoon and active site residues in sticks. Left panels use the m^{3}T coordinate as in the FTO crystal structure (PDB ID: 3LFM) to prepare the initial location of the base in the FTO simulation through the following steps: fix the sugar ring position in 3LFM and mutate m^{3}T to m^{3}C, m^{6}A, and hm^{6}A, respectively. Right panels use the base coordinates from aligned AlkB crystal structures (PDB ID: 3O1P for εA, and 3O1O for m^{3}T): align FTO and AlkB, take the aligned positions of m^{3}T and εA as the starting point and mutate εA to m^{6}A and hm^{6}A, respectively.

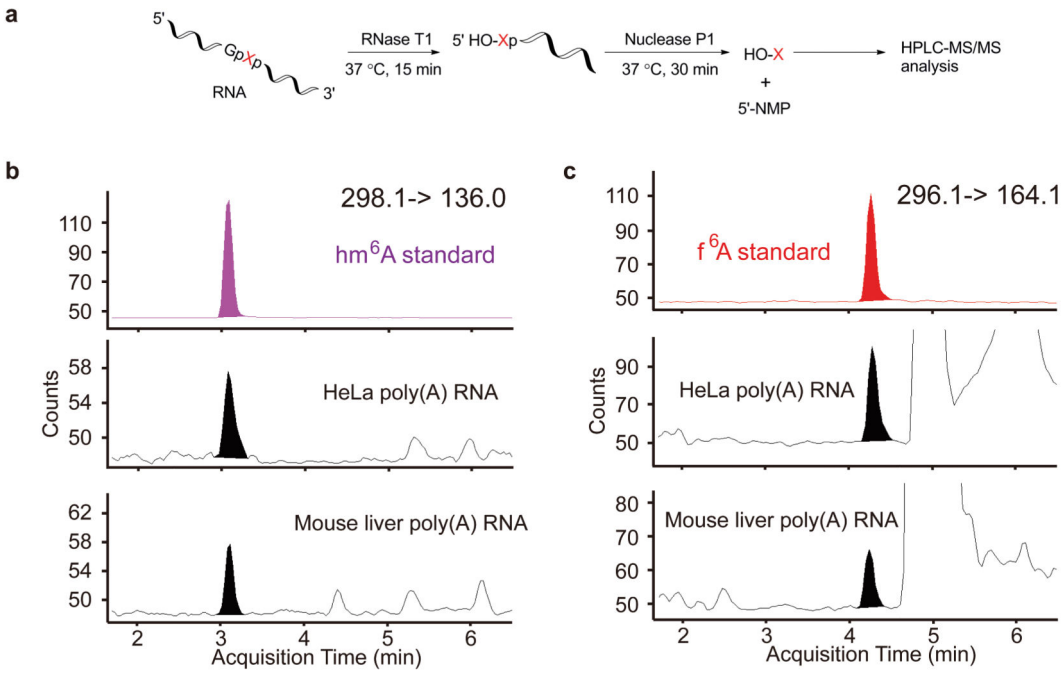

Figure 4. Presence of hm^6 A and f^6 A in mammalian mRNA

(**a**) Detection strategy: RNA is first digested with RNase T1 to expose the 5′ OH group of the base after G. Subsequent Nuclease P1 digestion releases the first base as nucleoside, and the rest of the bases as nucleoside 5′-monophosphate (5′-NMP). (**b, c**) LC-MS/MS analysis of digested mRNA isolated from HeLa cell and mouse liver samples showing the presence of hm^{6}A (**b**, 298.1->136.0, 3.1 min) and f^{6}A (**c**, 296.1->164.1, 4.2 min).

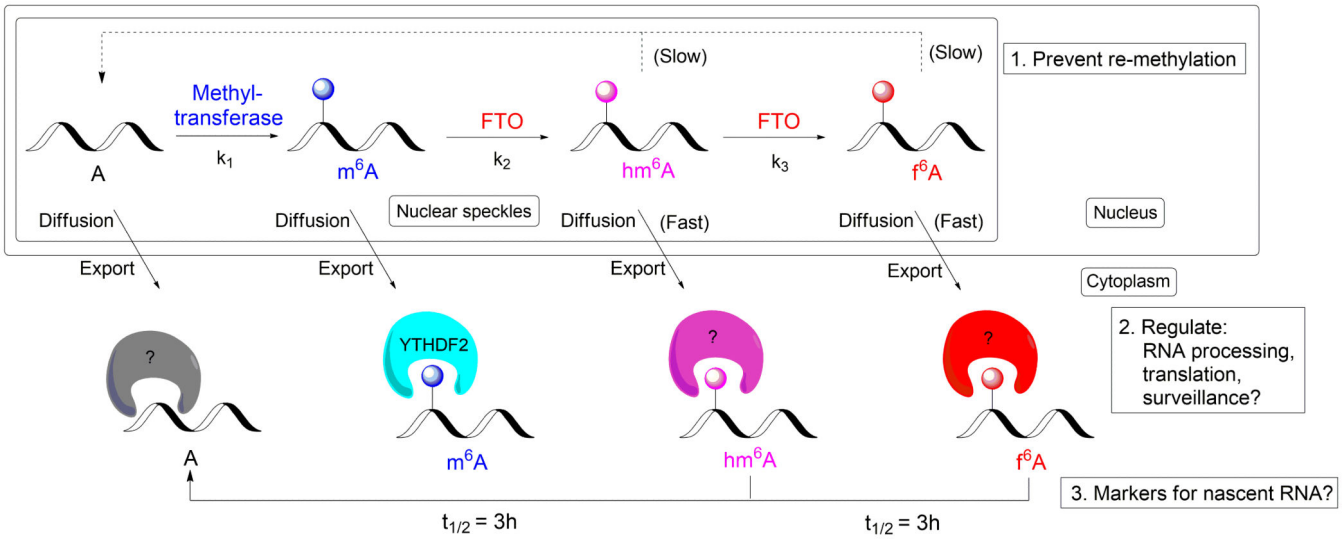

Figure 5. A proposed model of dynamic regulation of RNA modifications by FTO

Instead of direct demethylation, a delayed model is proposed for FTO, which possesses different kinetic behavior in order to accommodate additional diffusion/export process and avoid direct re-methylation. The nascent transcribed RNA is partially methylated by methyltransferase to m^6A. m^6A is converted to hm^6A in regions with low FTO levels, and to f^6A in regions with high FTO levels. Demethylated A is produced after the decomposition of hm^6A and f^6A, which is slower than the diffusion/export process, and which may help to avoid the re-methylation by methyltransferase at the nuclear speckles. When RNA is processed and exported to cytoplasm, different modifications on mRNA can potentially recruit or repel different protein factors, which could affect the metabolisms of mRNA. hm^6A and f^6A in RNA will eventually be hydrolyzed to A; these modifications may also serve as markers for nascent RNA.